Computers and Concrete, *Vol. 14 No. 1 (2014) 91-107*
DOI: http://dx.doi.org/10.12989/cac.2014.14.1.091

Cementing failure of the casing-cement-rock interfaces during hydraulic fracturing

Hai Y. Zhu[*1,2], Jin G. Deng[2a], Jun Zhao[3], Hu Zhao[3], Hai L. Liu[2] and Teng Wang[1]

[1]*State Key Laboratory of Oil & Gas Reservoir Geology and Exploitation, Southwest Petroleum University, Chengdu 610500, China*
[2]*State Key Laboratory of Petroleum Resource and Prospecting (China University of Petroleum, Beijing), Beijing 102249, China*
[3]*Oilfield Chemicals R & D Institute,COSL,Beijing East Yanjiao,065200,China*

(*Received October 19, 2013, Revised May 10, 2014, Accepted May 20, 2014*)

Abstract. Using the principle of damage mechanics, zero-thickness pore pressure cohesive elements (PPCE) are used to simulate the casing-cement interface (CCI) and cement-rock interface (CRI). The traction-separation law describes the emergence and propagation of the PPCE. Mohr-coulomb criteria determines the elastic and plastic condition of cement sheath and rock. The finite element model (FEM) of delamination fractures emergence and propagation along the casing-cement-rock (CCR) interfaces during hydraulic fracturing is established, and the emergence and propagation of fractures along the wellbore axial and circumferential direction are simulated. Regadless of the perforation angle (the angle between the perforation and the max. horizontal principle stress), mirco-annulus will be produced alonge the wellbore circumferential direction when the cementation strength of the CCI and the CRI is less than the rock tensile strength; the delamination fractures are hard to propagate along the horizontal wellbore axial direction; emergence and propagation of delamination fractures are most likely produced on the shallow formation when the in-situ stresses are lower; the failure mode of cement sheath in the deep well is mainly interfaces seperation and body damange caused by cement expansion and contraction, or pressure testing and well shut-in operations.

Keywords: delamination fractures; cement; interface; hydraulic fracturing; failure

1. Introduction

According to the statistics of China National Petroleum Corporation (CNPC), during 2000 to 2007 years, the CNPC had drilled 2378 gas wells. The Sustainable Annular Pressure (SAP) occured in many of these wells. Eleven of the thirteen wells in Kela gas field of Tarim basin experienced SAP to some extent. The SAP varied from 3.4 to 20MPa; Ten of the thirty-eight high sour gas wells at the Northeast of sichuan also experienced SAP, and the pressure range of the SAP was 0.26-20Mpa; the SAP which varied from 2.4 to 40 Mpa occurred in two of the six high sour gas wells in Chongqing province; the SAP also took place at Longgang-1 well, Longgang-2

∗Corresponding author, Ph.D., E-mail: zhuhaiyan040129@163.com
[a]Professor, E-mail: dengjingen@126.com.

http://www.techno-press.org/?journal=cac&subpage=8 ISSN: 1598-8198 (Print), 1598-818X (Online)

well, Longgang-3 well, Xushen-10 well, and Xushen-901 well. So, we can see that the SAP is very serious in oil & gas drilling industry.

In order to maintain the wellbore stability and protect the reservoir in drilling process (Zhu *et al*. 2013b), drilling fluid needs to have a certain plugging performance and wall building properties, which can produce a layer of mud cake in the wellbore wall to maintain the stability of the wellbore and reduce the leakage of fluid into the formation. The mud cake will decrease the cementing strength of cement and rock, and increase the cementing failure risk of the CCI during hydraulic fracturing. In field exploitation process, the formation pore pressure decreases, and the rock deformation increases due to the larger matrix stress. The cementing strength would also decrease due to the borehole fluid erosion. Additionally, the pressure test, well shutdown etc. operations will speed up the cement failure process. Gas leakage may be evidenced some years or decades later. So, cementing failure is mainly caused by interface departure and the cement breaking, which are caused by pressure test, well shutdown, cement expansion and shrinkage and so on. The micro-annulus around wellbore accelerates the propagation of the pre-fractures caused by well operation and cement deformation, and links up the two disconnected fractures.

When the casing-cement interface (CCI) and cement-rock interface (CRI) are failure to sealing the casing and formation, the SAP is most likely happened. The change of the formation condition and in the post-operating process will lead to the change of the stress-strain state of the CCR system, and thus may cause the cement sheath to lose its sealing capacity. For an offshore well, the oil & gas will leak off into the sea water which leads to some environmental problem.

The mechanism of the cement failure is complex and also one of the basic problems in the cementing engineering. Many scholars have studied this problem for many years. Previous reseach reveals that the failure model of the cement sheath includes the failure of the cement sheath and the cementing failure of the CCI and the CRI (Goodwin and Crook 1992; Heathman 2006; Urraca and Balázs 2009). According to the in-situ condition of the bottom-hole, the stress state of the cement sheath is extremely complex, so the analytic models based on certain assumptions can not analyze the process of the cumulated plastic damage of the cement sheath in the life-of-well (Thiercelin *et al*. 1998). To study the stress state of the cement sheath more accurately, Fleckenstein *et al*. (2000) pointed out that finite element method is the best way to solve the problem of cement failure. Ravi *et al*. (2002a, b) studied the stress state (radial and circumferential stresses) and the relevant failure model with the DIANA software. They reveal that the stress and displacement alonge the wellbore radial direction are not continuous because of the difference mechanical properties between the formation, cement sheath and casing. Two kinds of cement failure mechanisms were well-simulated in his study. Rodriguez *et al*. (2003) used the ANSYS software to analyze the two-dimensional plain strain problem of the CCR system with the assumptions that the cement sheath was well-cemented with casing and formation and that the in-situ stress is uniform. Pattillo and Kristiansen (2002) and Gray *et al*. (2009) simulated the stress states of the CCR system considering the drilling and post-operating processes, and predicted the integrality of the CCR system. These studies are all focus on the failure modes of the cement sheath, the CCI and the CRI during well test or the other production operations. Wang and Dahi (2012) firstly simulated the delamination fractures initiation and extension caused by excessive pore pressure and formation permeability considering the fractures as two zero thickness cohesive element layers. The cementing failure of the CCI and the CRI during hydraulic fracturing is still lack of research.

In recent years, some numerical calculation methods including finite element method (Jin *et al*. 2012; Jin and Shah 2013; Wang and Dahi Taleghani 2012), finite difference method (Nagel and

Sanchez-Nagel 2011), the boundary element method (BEM) (Hossain and Rahman 2008; Rahman *et al*. 2002), displacement discontinuity method (DDM) (Zhang *et al*. 2009), the discrete element method (DEM) (Nagel and Sanchez-Nagel 2012) and the extended finite element method (XFEM) (Taleghani 2009) are used to calculate initiation and propagation of fractures. The existing computing softwares for fracture initiation and propagation are: FLAC^{3D} (Nagel and Sanchez-Nagel 2011), FRANC^{3D} (Rahman *et al*. 2002), HYFRANC^{3D} (Hossain and Rahman 2008), RFPA (Tang *et al*. 2002), Abaqus (Chen *et al*. 2009; Zhang *et al*. 2010), UDEC/3DEC (Nagel and Sanchez-Nagel 2011, 2012) and so on. The XFEM can describe the non-plane fracture propagation behavior due to a specific in-situ stresses. Taleghani (2009) devoloped a XFEM code to simulate hydraulic fracture propagation in fractured reservoirs. Gordeliy and Peirce (2013) used the XFEM to solve the propagation problem of a plane hydraulic fracture in an elastic medium. Chen (2013) introduced a new finite element to Abaqus to incorporate the XFEM for the solution of hydraulic fracture problem. Using PPCE, hydraulic fracturing modules of Abaqus software simulates hydraulic fractures initiation and propagation as well as hydraulic fracturing fluid flow within the fractures. Chen *et al*. (2009) simulated two-dimensional radial fracture initiation and propagation problems using the PPCE, and the simulation results are fully consistent with analytical solution of K-vertex. Plastic formation hydraulic fracturing problems is simulated by Yao *et al*. (2010) using PPCE, and the results calculated from Abaqus is closer to the analytical solution than that calculated from P3D model and PKN model. Zhang *et al*. (2010) considered the effects of casing, cement sheath, micro annulus and perforation holes on three-dimensional hydrualic fracture, studied the fracture propagation mechanism in horizontal wells.

In this paper, we study the propagation of specific fractures along the casing-cement-rock interfaces during hydraulic fracturing, that is to say, the potential propagation pathes of the delamination cracks are known. So, the PPCE in Abaqus software can be used to solve this problem. Two zero thickness cohesive element layers are used to simulate the emergence and propagation of fractures along the wellbore axial and circumferential direction, the FEMs of fractures propagation along CCR interfaces in hydraulic fracturing are established. Mohr-coulomb criteria is used to describe the plastic behavior of cement sheath and rock. The mechanism of the cementing failure is simulated, which can be used to guide the well cementation design.

2. Design of laboratory hydraulic fracturing experiments with oriented perforating technique

2.1 The basic equations

2.1.1 Coupled nonlinear flow-stress equations

Fluid flow obeys the fluid continuity equation, and the rock mechanical properties are simulated by constitutive model defined by effective stress, the constitutive behavior of the fluid follows Darcy's law.

The relationship between effective stress and total stress is as follows:

$$\bar{\sigma} = \sigma + p_w I \tag{1}$$

where $\bar{\sigma}$ is the effective stress matrix; σ is the total stress matrix; I is the second-order unit tensor, p_w is the absolute value of pressure.

The control volume is V, its surface area is S, the rock matrix stress equilibrium equation is (Zhu *et al*. 2013):

$$\int_V \delta\dot{\varepsilon}^T \sigma \mathrm{d}V = \int_{S_\sigma} \delta v^T t \mathrm{d}S + \int_V \delta V^T \hat{f} \mathrm{d}V \tag{2}$$

where σ is the stress matrix; $\delta\dot{\varepsilon}$ is the virtual strain rate matrix; t is surface force vector; $\hat{f}$ is the body force vector and δv is the virtual velocity vector.

The stress equilibrium equation is discretized to get the finite element mesh of solid-phase material, so the fluid can flow through these meshes. Fluid flow should satisfy the continuity equation:

$$\frac{1}{J}\frac{\partial}{\partial t}(J\rho_w n_w) + \frac{\partial}{\partial x}(\rho_w n_w v_w) = 0 \tag{3}$$

where J is the volume ratio of porous medium; ρ_w is fluid density; n_w is void ratio; v_w is fluid seepage velocity; x is space vector. Fluid seepage velocity obeys Darcy's law:

$$v_w = -\frac{1}{n_w g \rho_w} J \cdot (\frac{\partial p_w}{\partial x} - \rho_w g) \tag{4}$$

where g is gravity acceleration, p_w is fluid flow. As can be seen from the above three equations, the rock matrix stress and pore fluid pressure are nonlinear coupled with each other to form a control equation. When it is converted into a weak form of the equivalent integral, it can be solved by the finite element discretization method.

The change in void ratio is due to the deformation of rock matrix. The relationship between porosity and volumetric strain is as follows:

$$n = 1 - \frac{1-n_0}{\varepsilon_{\mathrm{v}}} \tag{5}$$

where n_0 is the initial porosity. The relationship between the permeability coefficient and porosity is as follows:

$$k = \frac{\rho g}{\mu}\frac{d^2}{180}\frac{n^3}{(1-n)^2} \tag{6}$$

where μ is the fluid dynamic viscosity coefficient; d is the solid particles diameter. Combining the above two equations, the relationship between permeability coefficient and volumetric strain can be expressed as (Zhu *et al*. 2013):

$$k / k_0 = [(\frac{1}{n_0})(1+\varepsilon_V)^3 - (\frac{1-n_0}{n_0})(1+\varepsilon_V)^{-1/3}]^3 \tag{7}$$

where k_0 is the initial permeability coefficient.

2.1.2 Viscoelastic continuum damage constitutive model of the PPCE

(1) Damage evolution model of the PPCE

The PPCE stiffness matrix can be expressed as:

$$\begin{Bmatrix} t_n \\ t_s \\ t_t \end{Bmatrix} = \frac{E(1-v)}{(1+v)(1-2v)} \begin{bmatrix} 1 & 0 & 0 \\ 0 & \dfrac{1-2v}{2(1-v)} & 0 \\ 0 & 0 & \dfrac{1-2v}{2(1-v)} \end{bmatrix} \begin{Bmatrix} \varepsilon_n \\ \varepsilon_s \\ \varepsilon_t \end{Bmatrix} \tag{8}$$

As shown in Fig. 1, the normal and two tangential directions of PPCE have the same damage mode. When the displacement difference of the upper and lower surfaces of PPCE is less than d_n^0 (the initial damage displacement of PPCE), the PPCE deformation is in elastic stage, and element stress increases with its displacement. When the stress reaches to the cementing strength t_n^0, the element starts to be in its damage stage. The displacement of cohesive element in damage softening stage is $d_n^0 \sim d_n^f$. At this stage, the stress which can be withstanded by PPCE decreases with displacement increasing. When the displacement increases to d_n^f, the element can not withstand the stress, and then it completely failed with the fracture opened.

Damage is assumed to initiate when a quadratic interaction function involving the nominal stress ratios (as defined in the expression below) reaches a value of one. This criterion can be represented as (Camanho and Davila, 2002):

$$\left\{\frac{\langle t_n \rangle}{t_n^0}\right\}^2 + \left\{\frac{t_s}{t_s^0}\right\}^2 + \left\{\frac{t_t}{t_t^0}\right\}^2 = 1 \tag{9}$$

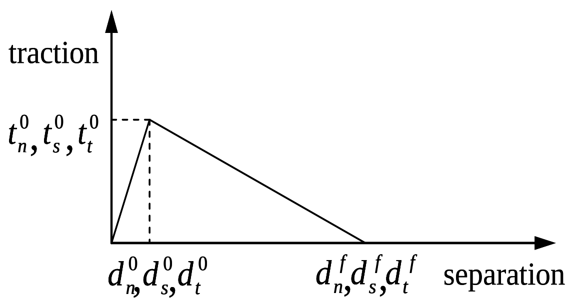

Fig.1 Traction-separation criterion of PPCE

where t_n^0 is tensile strength of PPCE, t_s^0 and t_s^0 are shear strength in two tangential directions.

PPCE damage evolution model is as follows:

$$\begin{cases} t_n = \begin{cases} (1-D)\bar{t}_n, & \bar{t}_n \geq 0 \\ \bar{t}_n, & \bar{t}_n < 0 \end{cases} \\ t_s = (1-D)\bar{t}_s \\ t_t = (1-D)\bar{t}_t \end{cases} \tag{10}$$

where $\bar{t}_n$, $\bar{t}_s$ and $\bar{t}_t$ are stresses in three directions of PPCE in undamaged stage with linear elastic deformation.

When Linear damage evolution criterion is selected, the damage factor is calculated as follows (Turon *et al*. 2006):

$$D = \frac{d_m^f (d_m^{\max} - d_m^0)}{d_m^{\max} (d_m^f - d_m^0)} \tag{11}$$

where $d_m^{\max}$ is the element maximum displacement; d_m^f is displacement when element is failure; d_m^0 is displacement when element damage starts.

(2) Fluid flow within cohesive element

Fluid within cohesive element flows along the normal (perpendicular to the upper and lower surfaces) and tangential directions, as shown in Fig. 2. Tangential flow is usually treated as Newtonian fluid and power law fluid. In this paper, power law fluid is selected to characterize the flow of the hydraulic fracturing fluid. Constitutive equation of the power-law flow is as follows:

$$\tau = K'\dot{\gamma}^{n'} \tag{12}$$

where τ is fluid tangential stress, $\dot{\gamma}$ is fluid tangential strain rate, K' is fluid consistency; n' is power-law coefficient.

The volume flow rate of tangential flow within cohesive element can be expressed as:

$$qd = \left(\frac{2n'}{1+2n'}\right)\left(\frac{1}{K'}\right)^{\frac{1}{n'}}\left(\frac{d}{2}\right)^{\frac{1+2n'}{n'}} \left|\nabla p\right|^{\frac{1-n'}{n'}} \nabla p \tag{13}$$

Normal flow within PPCE appears in the form of fluid loss from the element upper and lower surfaces. Fluid flow on the element upper and lower surfaces can be expressed as:

$$\begin{cases} q_t = c_t(p_i - p_t) \\ q_b = c_b(p_i - p_b) \end{cases} \tag{14}$$

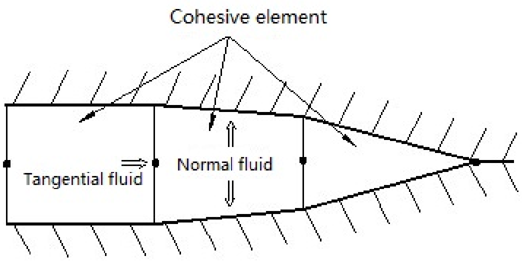

Fig. 2 Flow within cohesive element

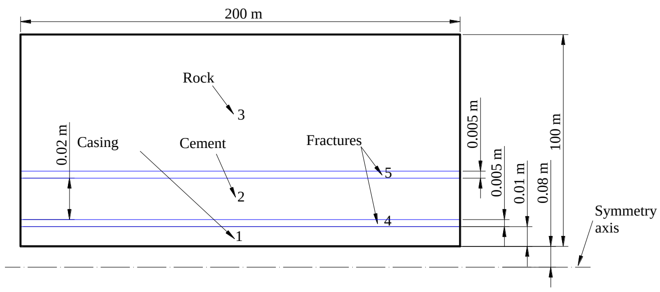

Fig.3 Geometry model of CCR system with delamination fractures

where q_t , q_b are volume flow rate on element upper and lower surfaces respectively; c_t , c_b are fluid loss coefficient on element upper and lower surfaces; q_t , q_b are seperately pore pressure on element upper and lower surfaces; p_i is fluid pressure within the element.

2.2 Modeling technology of axial delamination fractures

Since the size of the geometric units of casing and cement is in the millimeter-scale, and the wellbore axial length and formation is in the meter-scale, the finite element discretization of CCR system is very hard (Zhu *et al*. 2013a). Some simplifies and assumptions: (1) only considering the fracture emergence and propagation along the CCI and CRI; (2) assuming that there is no micro-annulus around the wellbore; (3) ignoring the hydraulic fracture propagation process, and few hydraulic fracturing fluid are used to initiate and propagate and propagation the delamination fractures during hydraulic fracturing. As seen in Fig. 3, the region “4” and “5” are used to simulate the CCI and CRI respectively. The axial size of the FEM is 200m, and the radial size is 100m. The wellbore diameter is φ 0.22m.

The problem is axisymmetric along the wellbore axis when the vertical stress and the maximum horizontal principal stress are equal. We use 127399 four-node axisymmetric, quadrilateral, reduced integration, hourglass control bilinear coupled displacements and pore pressure elements CAX3RP to mesh cement and formation rock, and use CAX3R to mesh the casing. Using sweep meshing technology, the region 4 and 5 are meshed by cohesive elements COHAX4, then a layer of pore pressure nodes are set in the middle of the cohesive elements to convert the cohesive elements into PPCE. Fig. 4 is the FEM of emergence and propagation of delamination fractures in the wellbore axial direction. 20087 PPCE COHAX4P are meshed for the fractures. The initial condition of the formation rock is saturated. The initial void ratio, permeability and the in-situ stress are also assigned to the FEM. The horizontal displacements of the left and right sides and the vertical movement of the upper side of the model is fixed, and the fluid hydrostatic pressureis applied to the inner casing.

2.3 Modeling technology of the micro-annlus fracture and hydraulic fracture

After the casing is cemented to the rock formation, a perforation gun is put into the bottomhole. Then a number of perforations is shoot by the perforating shaped charge around the wellbore. The perforations provide the flow paths of hydraulic fracturing from wellbore to the oil & gas bearing formation. During the process of hydraulic fracturing, it is the hydraulic fracturing fluid that has directly caused the tunnel wall to fracture.

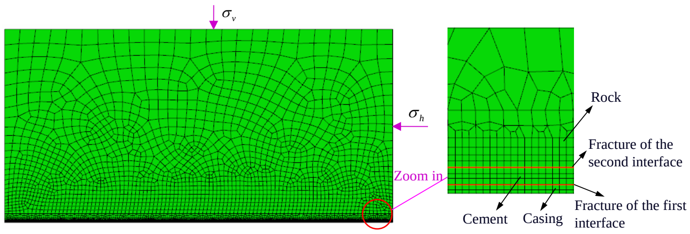

Fig. 4 FEM of emergence and propagation of delamination fractures

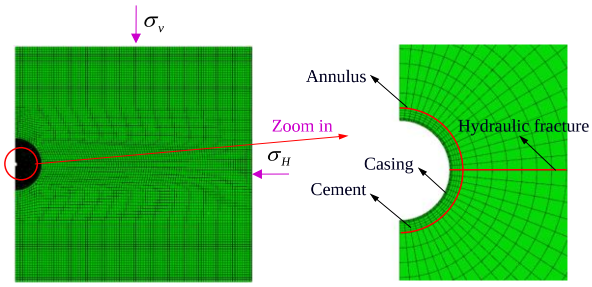

Fig. 5 Micro-annulus around wellbore

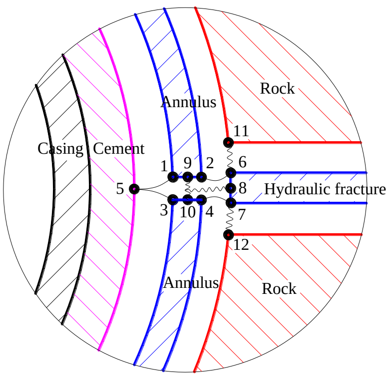

Fig. 6 Modeling technology of the micro-annlus fracture and hydraulic fracture

Economides and Nolte (1991) pointed out that the fracturing fluid will flow around the wellbore (producing a micro-annulus) if the hydraulic fracture initiation point is not along the perforations, and the hydraulic fracture will initiate in the most likely initiation point which locates in the direction of the maximum horizontal principal stress. When the perforation orientation is not consistent with the maximum principal stress, the micro-annulus is likely to increase the fracturing fluid's pressure drop near wellbore, and improves the formation initiation pressure.

To study the mechanism of micro-annulus initiation and propagation in hydraulic fracture process, a FEM of circumferential fracture initiation and propagation along the CCI is established (Fig. 5). And the model size is 200m×200m. The boundary conditions are: (1) Model’s left border has symmetry constraints; (2) the horizontal displacement of the right border is fixed, (3) the vertical displacement of the upper and lower sides is fixed, (4) the upper and lower sides and right border are applied with in-situ pore pressure; (5) nodes of the entire model are applied with the in-situ stresses, pore pressure, porosity and saturation. "Tie nodes" modeling technology is used because it is difficult to establish an annular PPCE directly. As shown in Fig. 6, the annulus PPCE and rock are divided into two parts, and the annulus PPCE and the hydraulic fracture PPCE are modeled individually. All of the fractures are meshed by COH2D elements using sweep meshing technology. The sweep direction of annulus fracture is from left to right, and the sweep direction of hydraulic fracture is from up to down. A layer of pore pressure nodes are also set in the middle of the cohesive elements to convert the cohesive elements into PPCE. Then, the intermediate pore pressure node 9 of the upper annulus fracture, node 10 of the lower annulus fracture, and node 8 of the hydraulic fracture are replaced with a same node to simulate fluid flow simultaneously in three directions at this point. Node 5 of the right cement side is tied to the node 1 and 3 of the upper and lower annulus fracture respectively. Node 2 and 4 of the annulus fracture are tied to node 6 and 7 of the hydraulic fracture respectively. Node 6 and 7 are tied to node 11 and 12 of the upper and lower part of the rock respectively. At the same time, the cohesive nodes at the upper and lower surfaces of hydraulic fracture are tied to the adjacent nodes of the rock, and the left and right sides nodes of the micro-annulus are tied respectively to the left side of cement nodes and right side of rock nodes.

3. Field application

3.1 Geometrical and mechanical parameters of cement, rock and casing

Take C7-well of the east C platform in South China Sea as the research object. The cement samples are treated as φ50 mm × 100 mm cylinders and the samples are tested by the MTS rock mechanics experiment device (Zhu *et al*. 2012). The experiment results are shown in Table 1. The cement cohesion is about 9.2MPa, and internal fraction angle is 28.6°. Tensile strength is measured using the Brazilian disc test, and results are shown in Table 2. The average tensile strength of cement samples is 2.2MPa. From the water permeability experiment, we found that the cement permeability is 1e-13m2, and porosity is 0.7%.

C7-well is the horizontal well drilled along the minimum horizontal principal stress direction, and the wellbore horizontal section is completed with tail casing. Perforating position is located at the depth of 4400 m. Well structure is shown in Table 3. The reservoir is located in the third

Table 1 The results of cementing cement rocks mechanics experiments

No.	Diameter (mm)	Length (mm)	Density (g/cm^3)	Confining pressure (MPa)	Strength (MPa)	Elastic modulus (MPa)	Poisson's ratio
1	25.18	49.40	1.73	0	22.437	5.699	0.151
2	25.12	48.69	1.73	0	19.269	6.7152	0.227
3	25.12	41.86	1.73	0	19.863	5.189	0.167
4	25.12	47.98	1.75	0	15.373	4.8105	0.148
5	25.18	49.39	1.72	0	19.482	5.7687	0.168
6	25.18	49.17	1.73	0	15.913	4.6694	0.151
7	25.12	48.00	1.73	0	28.34	5.022	0.180
8	25.18	49.07	1.73	5	43.616	5.5566	0.152
9	24.82	48.83	1.64	5	43.62	5.395	0.187
10	24.98	48.45	1.57	10	62.67	7.150	0.191
11	25.12	47.99	1.73	15	72.01	7.967	0.193

Table 2 Cement sample tensile test results

No.	Diameter (mm)	Thickness (mm)	Breaking stress (KN)	Tensile strength (MPa)
1	24.97	6.91	0.557	2.05
2	24.97	6.56	0.601	2.33
3	24.97	6.87	0.524	1.94
4	25.01	7.42	0.876	3.00
5	25.01	7.03	0.801	2.90
6	25.01	7.09	0.815	2.93
7	25.02	6.69	0.398	1.51
8	25.02	6.68	0.435	1.66
9	25.02	6.95	0.412	1.51

Table 3 Casing structure of C7 well

Wellbore size (in)	Inclined depth (m)	Vertical depth (m)	Casing depth (m)	Casing size
Drilling riser		209.50	209.50	24"
17-1/2	1605.00	1600.00	1600.00	13-3/8"
12-1/4	4005.00	3212.00	4000.00	9-5/8"
8-1/2	5063.00	3212.00	3850.00~5058.00	7"

section of Zhuhai formation, and it is a positive fault formation. The vertical stress and maximum horizontal stress are both 63.8 MPa, the minimum horizontal stress is 51.5MPa, and the pore pressure is 36.5MPa. During the fracturing process, the fracturing fluid has a density of 1250 Kg/m^3, its viscosity is 0.1Pas and its displacement is $0.24m^3/min$. The elastic modulus of the rock formation is 14.6 GPa, the Poisson's ratio is 0.14, the permeability rate is 2e-10 m^2, porosity is 11%, density is 2600 Kg/m^3, the cohesive strength is 12Pa, the internal friction angle is 26°, and the tensile strength is 5.8 MPa. Casing elastic modulus is 210GPa and its Poisson's ratio is 0.21.

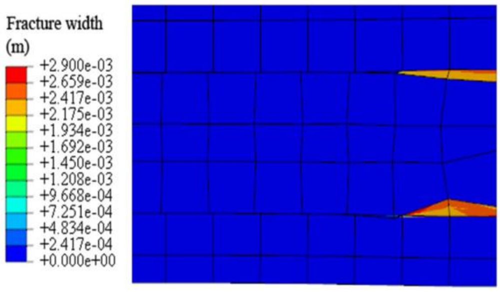

Fig. 7 Fracture width

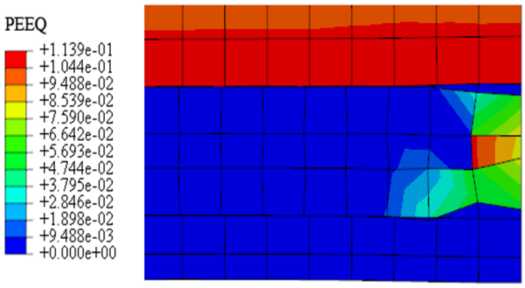

Fig. 8 Equivalent plastic strain of cement and rock

3.2 Fracture emergence and propagation along wellbore axis during hydraulic fracturing

3.2.1 Fracture emergence and propagation of the CCI and CRI simultaneously

The fracture width along axial wellbore in horizontal well and the equivalent plastic strain of cement and rock, are as shown in Fig. 7 and Fig. 8 respectively. We can conclude that: (1) the nonlinearity of the model is very high, and the calculation amount is large when two delamination fractures propagate simultaneously; (2) fracture width is large and difficult to propagate further. As the hydraulic fracturing continues, the fracture width increases, but the fracture length is hard to grow; (3) The plastic deformation of cement and the fracture tip is very strong. Plastic flow leads to strong choking effect, resulting that the fractures are hard to open.

3.2.2 Fracture emergence and propagation of the CCI

We set a layer of PPCE along the CCI. The cement and rock share the same nodes at their interface. The geometric parameters and boundary conditions of this model is the same as that of FEM considering the CCI and CRI fractures simultaneously.

Only considering the fracture emergence and propagation of the CCI, fracture width is shown in Fig. 9. The fracture width is uniform. The fracture tip width has a slight increasing, which is caused by the plastic strain of fracture tip (Fig. 10). The large plastic flow area restrains the fracture propagation. The relationship between the fracture length along wellbore axis and the fracturing time is shown in Fig. 11. The fracture grows steadily and the fracture length is proportional to the fracture time. The fracture growing velocity is about 7m/min. In fact, this situation cannot exist. For a horizontal well in the direction of minimum horizontal principal stress, the fracture initiation pressure can be expressed as:

$$p_f = 3\sigma_H - \sigma_v - P + S_t \tag{15}$$

According to the in-situ conditions of the C7-well, the fracture initial pressure is 96.9MPa. Seen from Fig. 12, the fracture propagation pressure increases gradually, and it is three times of the fracture initiation pressure. Actually, this situation can not happen during hydraulic fracturing process. A typical hydraulic fracturing curve seen in Fig. 13 (Zhu *et al*. 2013), during hydraulic fracturing, the bottom-hole pressure firstly increases to the rock fracture pressure, and then the fracture propagates away from the bottom-hole. The bottom-hole pressure will maintain at a certain pressure during fracture prapagation. The fracture propagation pressure is lower than the fracture initiation pressure, which illustrates that the CCI fracture can hardly propagate along wellbore axis.

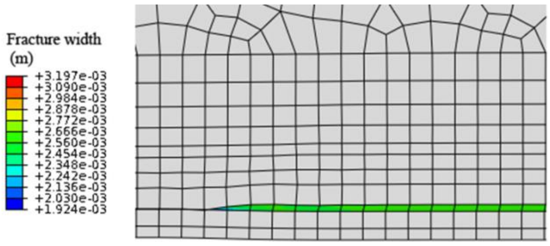

Fig. 9 Fracture aperture

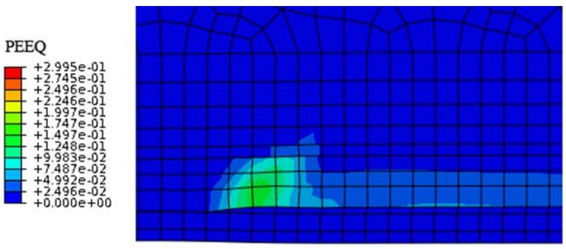

Fig. 10 Equivalent plastic strain of cement and rock

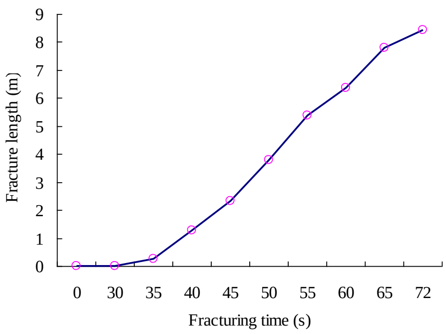

Fig. 11 The relationship between the fracture length and the fracturing time

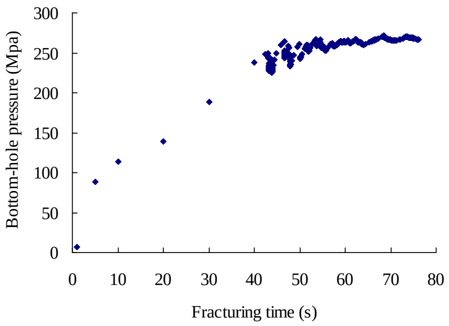

Fig. 12 The relationship between the bottom-hole pressure and the fracturing time

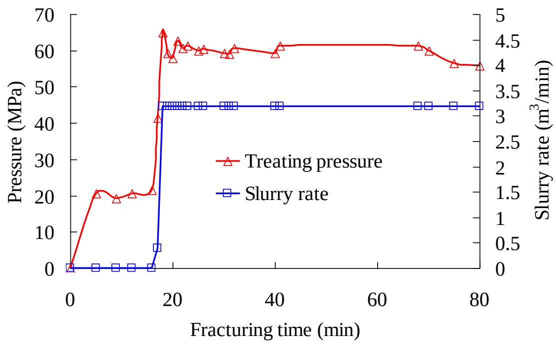

Fig. 13 The filed hydraulic fracturing operation curve of an oil-well (Zhu *et al*. 2013)

3.3 Fracture emergence and propagation along wellbore circumference during hydraulic fracturing

(1) If the perforation direction is 90° from the maximum horizontal principal stress, the fracture width of the micro-annulus and hydraulic fracture is calculated in Fig. 14. The realationgship between the bottom-hole pressure and the fracture time at the 90° and 0° perforation angle are shown in Fig. 15. When the cementing strength is lower than the tensile strength of the rock formation, the micro-annulus can emergence and propagation quickly, and the initial pressure of micro-annulus fracture is 0.05MPa higher than that of hydraulic fracture. The restrict zone limits the fluid’s flow around the wellbore, and the throttling effect exists to cause the pressure decreasing. This will increase the bottom-hole pressure and the sand screening risk. The width of the throtting channel produced in the entrance of the hydraulic fracture is $w^2/8D$ (Economides and Nolte, 1991), where the D is wellbore diameter.

(2) If the perforation angle is 0°, the fracture width of the micro-annulus and hydraulic fracture is shown in Fig. 16. Although the cementing strength is lower than the rock tensile strength, the micro-annulus also emerges and propagates. The bottom-hole pressure increases after the emergeing of the micro-annulus, and then hydraulic fracture starts to initiate. The micro- annulus grows around the wellbore no matter what the direction of perforation is. Under the same

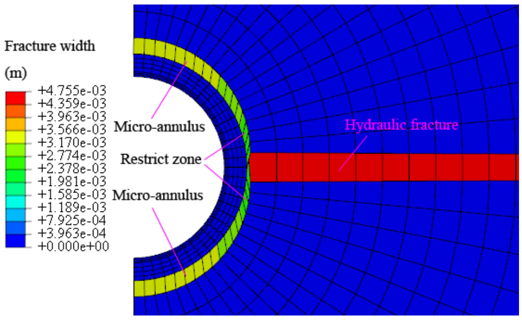

Fig. 14 Fracture width of the micro-annulus and hydraulic fracture at 90° perforation angle

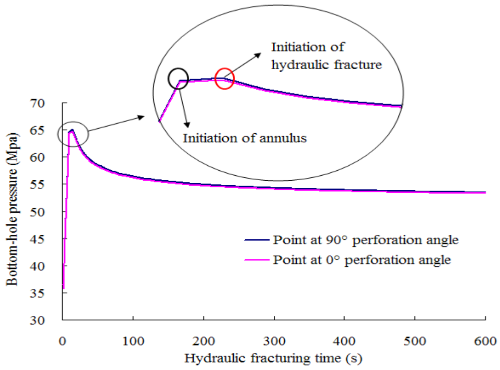

Fig. 15 The realationgship between BHP and fracture time

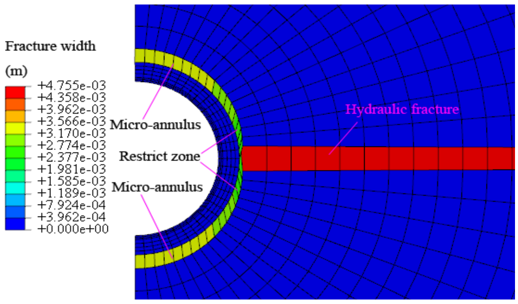

Fig. 16 Fracture width of the micro-annulus and hydraulic fracture at 0° perforation angle

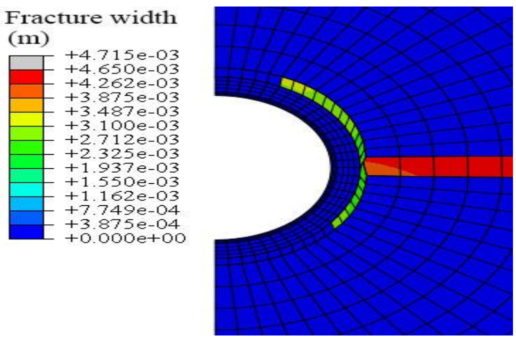

Fig. 17 Micro-annulus when the stress difference is larger than 20MPa

conditions, the width of micro-annulus in 0° perforation is almost the same as that in the 90°perforation, that is due to the smaller stress difference between the max. and min. horizontal principle stresses (63.8-51.5 = 12.3 MPa).

When the stress difference between the max. and min. horizontal principle stress is larger than 20MPa, the micro-annulus width of the 90°perforation is larger than the 0° perforation, and the micro-annulus is different to generate (Fig. 17).

3.4 Results and discussion

(1) The axial fractures of CCI and CRI are hard to propagate at the same, because the plastic deformations of cement and the fracture tip restrict the fracture propagation.

(2) Only considering the CCI fracture, the fracture grows steadily and the fracture length is proportional to the fracture time, and its growing velocity is about 7 m/min. Actually, the bottom-hole pressure increases nonlinearly during hydraulic fracturing. When the hydraulic fracture initiation pressure of the rock formation is lower than the CCI fracture initiation pressure, the hydraulic fracture firstly initiates and propagates, and then the bottom-hole pressure decreases to the hydraulic fracture propagation pressure. The bottom-hole pressure can't increase to the initiation pressure of the CCI fracture. So, for a deep horizontal well, the delamination fractures are hard to generate, which verifies the Dusseault *et al*. (2000)'s results "Emergence and propagation of delamination fractures generate in the vertial well of shallow formations where the in-situ stress and pore pressure are not too large or the old oilfied where the formation pressure is much smaller." indirectly.

(3) When the cementing strength of the CCI and CRI is lower than the rock tensile strength, the micro-annulus emerges and propagates no matter what the direction of perforation is. So, the circumferential stress in uncased well should be used to calculate the fracture initiation pressure in hydraulic fracturing if the cementing strength is lower than that of the rock formation.

(4) Seidel and Greene (1985) point out that "A micro-annulus of only 0.001" (0.025 mm) is sufficient to give gas a flow path". When the gap between the cement sheath and the casing reaches to 0.025 mm, the fracturing fluid with high viscosity can't always pass. It means that the fracturing fluid cannot always flow as we think about it. Dusseault *et al*. (2000) also pointed out that the wellbore gas would go up to the well surface when the gap of CCR system is about 10-20 μm. The micro-annulus around the wellbore is hard to propagate along the wellbore axis in the well horizontal section during hydraulic fracturing. Although the micro-annulus doesn't generate in the horizontal well, the cement need to have a strong plastic property to avoid the debonding between the cement and the casing.

4. Conclusions

Using the viscoelastic continuum damage mechanics, the FEM models of the emergence and propagation of delamination fractures are proposed. Delamination fractures are hard to generate in horizaontal well during hydraulic fracturing happen, the cementing failure of the cement in a horizontal well is caused by the pressure changeable inside the wellbore during drilling and completion operation. When the cementing strength of the CCI and CRI is lower than the rock tensile strength, the micro-annulus emerges and propagates no matter what the direction of perforation is. When the stress difference between the max. and min. horizontal principle stress is larger than 20MPa, the micro-annulus width of the 90°perforation is larger than the 0° perforation, and the micro-annulus is different to generate.

Acknowledgments

This work was supported by the SWPU Science & Technology (No. 2013XJZ003) and Academic Fund, the research Foundation of Sichuan Province under Grant No. 2014HH0004 and the National Natural Science Foundation of China (No. 51374178, 51221003, 51174219) and the Key Program of National Natural Science Foundation of China (No. 51134004). This work was also supported by the National Basic Research Program of China (973 Program, No. 2014CB239205).

References

Camanho, P.P. and Davila, C.G. (2002), “Mixed-mode decohesion finite elements for the simulation of delamination in composite materials”, *NASA/TM-2002-211737*, 1-42.

Chen, Z.R. (2013), “An ABAQUS implementation of the XFEM for hydraulic fracture problems”, In: “*Effective and Sustainable Hydraulic Fracturing*”, Eited by Bunger, A.P., McLennan, J. and Jeffrey, R., Publisher: InTech, May 17, 725-739.

Chen, Z., Bunger, A.P., Zhang, X. and Jeffrey, R.G. (2009), “Cohesive zone finite element-based modeling of hydraulic fractures”, *Acta Mech. Solida Sin.*, **22**(05), 443-452.

Dusseault, M.B., Gray, M.N. and Nawrocki, P.A. (2000), “Why oilwells leak: cement behavior and long-term consequences”, *SPE International Oil and Gas Conference and Exhibition*, Beijing, China.

Economides, M.J. and Nolte, K. (1991), *Reservoir Stimulation*, second edition. Englewood Cliffs, New Jersey: Prentice–Hall, Inc.

Fleckenstein, W.W., Eustes, AW. and Miller, M.G. (2000), “Burst induced stresses in cemented well bores”, *SPE/AAPG Western Regional Meeting*, Long Beach, California.

Goodwin, K.J. and Crook, R.J. (1992), “Cement sheath stress failure”, *SPE Drilling Engineering*, December, 291-296.

Gordeliy, E. and Peirce, A. (2013), “Coupling schemes for modeling hydraulic fracture propagation using the XFEM”, *Comput. Method. Appl. Mech. Eng.*, **253**, 305-322.

Gray, K.E., Podnos, E. and Becker, E. (2009), “Finite-element studies of near-wellbore region during cementing operations: Part I”, *SPE Drilling Completion*, March, 127-136.

Hossain, M.M. and Rahman, M.K. (2008), “Numerical simulation of complex fracture growth during tight reservoir stimulation by hydraulic fracturing”, *J. Petrol. Sci. Eng.*, **60**, 86-104.

Jin, X., Shah, S.N. and Sheng, M. (2012), “Hydraulic fracturing model based on nonlinear fracture mechanics: theory and simulation”, *SPE Annual Technical Conference and Exhibition*, San Antonio, Texas, USA.

Jin, X. and Shah, S.N. (2013), “Fracture propagation direction and its application in hydraulic fracturing”, *SPE Hydraulic Fracturing Technology Conference*, The Woodlands, TX, USA.

Nagel, N.B. and Sanchez-Nagel, M. (2011), “Stress shadowing and microseismic events: A numerical evaluation”, *SPE Annual Technical Conference and Exhibition*, Denver, Colorado, USA.

Nagel, N.B., Sanchez-Nagel, M. and Lee, B. (2012), “Gas shale hydraulic fracturing: A numerical evaluation of the effect of geomechanical parameters”, *SPE Hydraulic Fracturing Technology Conference*, The Woodlands, Texas, USA.

Pattillo, P.D. and Kristiansen, T.G. (2002), “Analysis of horizontal casing integrity in the valhall field”, *SPE/ISRM Rock Mechanics Conference*, Irving, Texas, USA.

Rahman, M.M., Hossain, M.M., Crosby, D.G., Rahman, M.K. and Rahman, S.S. (2002), "Analytical, numerical and experimental investigations of transverse fracture propagation from horizontal wells", *J. Petrol. Sci. Eng.*, **35**(3-4), 127-150.

Ravi, K., Bosma, M. and Gastebled, O. (2002a). "Safe and economic gas wells through cement design for life of the well", *SPE Gas Technology Symposium*, Calgary, May.

Ravi, K., Bosma, M. and Gastebled, O. (2002b), "Improve the economics of oil and gas wells by reducing the risk of cement failure", *IADC/SPE Drilling Conference*, Dallas, February.

Rodriguez, W.J., Fleckenstein, W.W. and Eustes, A.W. (2003), "Simulation of collapsed load on cemented casing using finite element analysis", *SPE Annual Technical Conference*, Denver, Colorado.

Seidel, F.A. and Greene, T.G. (1985), "Use of expanding cment improves bonding and aids in eliminating annular gas migration in hobbs grayburg-san andres wells", *SPE Annual Technical Conference and Exhibition*, Las Vegas, Nevada, September.

Taleghani, A.D. (2009), "Analysis of hydraulic fracture propagation in fractured reservoirs: an improved model for the interaction between induced and natural fractures", Ph. D Dissertation, The University of Texas at Austin.

Tang, C.A., Tham, L. G., Lee, P.K.K., Yanga, T.H. and Lia, L.C. (2002), "Coupling analysis of flow, stress and damage (FSD) in rock failure", *Int. J. Rock Mech. Mining Sci.*, **39**(4), 477-489.

Thiercelin, M., Baumgarte, C. and Guillot, D. (1998) "A Soil Mechanics Approach To Predict Cement Sheath Behavior", *SPE/ISRM Rock Mechanics in Petroleum Engineering Conference*, Trondheim, Norway, July.

Turon, A., Camanho, P.P., Costa, J. and Davila, C.G. (2006), "A damage model for the simulation of delamination in advanced composites under variable-model loading", *Mech. Mater.*, **38** (11), 1072-1089.

Urraca, M. and Balázs, I. (2009), "Targeting Zonal Isolation Challenges on the Strategic Szoreg UGS Project, Hungary", *SPE/IADC Middle East Drilling Technology Conference & Exhibition*, Manama, Bahrain, October.

Wang, W. and Dahi, T. A. (2012), "Emergence and Propagation of Delamination Fractures along the Casing-Cement Interface", *46th US Rock Mechanics / Geomechanics Symposium*, Chicago, IL, USA, June.

Xue, B., Wu, H.A., Wang, X.X., Lian, Z.L., Zhang, J. and Zhang, S.C. (2006), "A three-dimensional finite element model of hydraulic progressive damage", *Key Eng. Mater.* 324-325, 375-378.

Yao, Y., Gosavi, S.V., Searles, K.H. and Ellison, T.K. (2010), "Cohesive Fracture Mechanics Based Analysis to Model Ductile Rock Fracture", *44th US Rock Mechanics Symposium and 5th U.S.-Canada Rock Mechanics Symposium*, Salt Lake City, UT, June.

Zhang, G.M., Liu, H., Zhang, J., Wu, H.A. and Wang, X.X. (2010), "Three-dimensional finite element simulation and parametric study for horizontal well hydraulic fracture", *J. Petrol. Sci. Eng.*, 72, 310-317.

Zhang, X., Jeffrey, R.G. and Thiercelin, M. (2009), "Mechanics of fluid-driven fracture growth in naturally fractured reservoirs with simple network geometries", *J. Geophys. Res.*, **114**, 402-406.

Zhu, H.Y., Deng, J.G., Chen, Z.J., An, F.C., Liu, S.J., Peng, C.Y., Wen, M. and Dong, G. (2013), "Perforation optimization of hydraulic fracturing of oil and gas well", *Geomech. Eng.*, **5**(5), 463-483.

Zhu, H., Deng, J., Xie, Y., Huang, K., Zhao, J. and Yu, B. (2012), "Rock mechanics characteristic of complex formation and faster drilling techniques in Western South China Sea oilfields", *Ocean Eng.*, **39**(44), 33-45.

Zhu, X.H., Liu, S.H. and Tong, H. (2013a), "Plastic limit analysis of defective casing for thermal recovery wells", *Eng. Fail. Anal.*, 27, 340-349.

Zhu, X.H., Tang, L.P. and Tong, H. (2013b), "Effects of high-frequency torsional impacts on rock drilling", *Rock Mech. Rock Eng.*, DOI: 10.1007/s00603-013-0461-0.

CC